Controlled Fluidization, Mobility, and Clogging in Obstacle Arrays Using Periodic Perturbations

C. Reichhardt and C. J. O. Reichhardt
Theoretical Division and Center for Nonlinear Studies, Los Alamos National Laboratory, Los Alamos, New Mexico 87545, USA

(Received 25 April 2018; published 7 August 2018)

We show that the clogging susceptibility and flow of particles moving through a random obstacle array can be controlled with a transverse or longitudinal ac drive. The flow rate can vary over several orders of magnitude, and we find both an optimal frequency and an optimal amplitude of driving that maximizes the flow. For dense arrays, at low ac frequencies, a heterogeneous creeping clogged phase appears in which rearrangements between different clogged configurations occur. At intermediate frequencies, a high-mobility fluidized state forms, and, at high frequencies, the system reenters a heterogeneous frozen clogged state. These results provide a technique for optimizing flow through heterogeneous media that could also serve as the basis for a particle separation method.

DOI: 10.1103/PhysRevLett.121.068001

Particle transport through heterogeneous media is relevant to flows in porous media [1,2], transport of colloidal particles on ordered or disordered substrates [3–7], clogging phenomena [8–13], filtration [14–16], and active matter motion in disordered environments [17–20]. It also has similarities to systems that exhibit depinning phenomena when driven over random or ordered substrates [21]. Recent work has focused on clogging effects for particle motion through obstacle arrays, where the onset of clogging is characterized by the formation of a heterogeneously dense state [11–13]. Such clogging is relevant for the performance of filters or for limiting the amount of flow through disordered media, so understanding how to avoid clog formation or how to optimize the particle mobility in obstacle arrays is highly desirable. Clogging also occurs for particle flow through hoppers or constrictions, where there can be a transition from a flowing to a clogged state as the aperture size decreases [22–26]. The clogging susceptibility in such systems can be reduced with periodic perturbations or vibrations [27–29]. Applied perturbations generally produce enhanced flows in disordered systems [30–34]; however, there are examples where the addition of perturbations or noise can decrease the flow or induce jamming, such as the freezing by heating phenomenon [26,35,36] or the appearance of a reentrant high-viscosity state in vibrated granular matter [37]. A natural question is whether clogging and mobility for particle flows through obstacles can be controlled or optimized with applied perturbations in the same way as hopper flow. It is also possible to have transverse shaking in hopper geometries [34], and it would be interesting to understand how transverse and longitudinal ac drives can control the flow in two-dimensional (2D) disordered obstacle arrays, where one type of shaking may be more effective than the other.

In this work, we numerically examine particle flow through a disordered obstacle array where the particles experience both a dc drive and ac shaking. In the absence of the ac shaking, this system exhibits a well-defined clogging transition at a critical obstacle density $\phi_c^{\rm dc}$ as identified in previous work [12] for dc-driven disks in obstacle arrays. The clogged states exhibit strong spatial heterogeneity, and $\phi_c^{\rm dc}$ remains roughly constant until the disk density approaches the jamming or crystallization density [12]. The previous work focused on the transition to a completely immobile state and the distinction between jamming and clogging behavior. In the present work, we measure the disk mobility when a transverse or longitudinal ac drive is added to the system for obstacle densities above $\phi_c^{\rm dc}$, where the ac drive serves to unclog the system. We find that the mobility drops back to zero above a critical obstacle density $\phi_c^{\rm ac}$ that depends on the frequency and amplitude of the ac drive. We identify an optimal ac frequency and amplitude that optimizes the mobility. At low frequencies the system forms a nearly immobile heterogeneous creeping clogged state, while for intermediate frequencies a more uniform flowing fluidized state appears, and at high frequencies a heterogeneous frozen clogged state emerges that resembles the clogged state under zero ac drive. These results indicate how to control the mobility of particles flowing through random disorder by applying dc and transverse or longitudinal ac drives to systems such as granular matter, colloids, or emulsions. Similar driving protocols could be used for particles with longer-range interactions such as superconducting vortices, Skyrmions, or charged colloids in disordered media to identify ac driving frequencies that optimize the flow.

Simulation and system.—We simulate a 2D system of nonoverlapping repulsive particles in the form of disks

interacting with a random array of obstacles in the form of posts, where the particles are subjected to a dc drift force and an ac shaking force. The sample is of size $L \times L$ with $L = 100$, and we impose periodic boundary conditions in the x and y directions. Interactions between pairs of disks i and j are given by the repulsive harmonic force $\mathbf{F}_{dd}^{ij} = k(r_{ij} - 2R_d)\Theta(r_{ij} - 2R_d)\hat{\mathbf{r}}_{ij}$, where the disk radius $R_d = 0.5$, $r_{ij} = |\mathbf{r}_i - \mathbf{r}_j|$, $\hat{\mathbf{r}}_{ij} = (\mathbf{r}_i - \mathbf{r}_j)/r_{ij}$, and Θ is the Heaviside step function. The spring stiffness $k = 200$ is large enough that disks overlap by less than 1%, placing us in the hard disk limit as confirmed by previous works [11,12,38]. The obstacles are modeled as immobile disks with the same radius and disk-disk interactions as the mobile particles. There are N_m mobile particles with an area coverage of $\phi_m = N_m \pi R_d^2/L^2$, while the area coverage of the $N_{\rm obs}$ obstacles is $\phi_{\rm obs} = N_{\rm obs}\pi R_d^2/L^2$, and the total area coverage is $\phi_{\rm tot} = \phi_m + \phi_{\rm obs}$. For monodisperse disks, the system forms a triangular solid at $\phi_{\rm tot} = 0.9$ [38]. The obstacles are placed in a dense lattice and randomly diluted until the desired $\phi_{\rm obs}$ is reached so that the minimum spacing between obstacle centers is $d_{\rm min} = 2.0$. The particle dynamics are governed by the following overdamped equation of motion: $\eta d\mathbf{r}_i/dt = \mathbf{F}_{\rm inter}^i + \mathbf{F}_{\rm obs}^i + \mathbf{F}_{\rm dc} + \mathbf{F}_{\rm ac}$. Here $\mathbf{F}_{\rm inter}^i = \sum_{j=0}^{N_m} \mathbf{F}_{dd}^{ij}$ are the particle-particle interactions, $\mathbf{F}_{\rm obs}^i = \sum_{k=0}^{N_{\rm obs}} \mathbf{F}_{dd}^{ik}$ are the particle-obstacle interactions, and $\mathbf{F}_{\rm dc} = F_{\rm dc}\hat{\mathbf{x}}$ is the dc drift force applied in the positive x direction, where $F_{\rm dc} = 0.05$. Each simulation time step is of the size $dt = 0.002$, and $\eta = 1.0$. Distances (forces) are measured in units of l_0 (f_0), and time is in units of $\tau_0 = \eta l_0/f_0$. We apply a sinusoidal ac drive that is either transverse, $\mathbf{F}_{\rm ac} = F_{\rm ac}^{\perp}\hat{\mathbf{y}}$, or longitudinal, $\mathbf{F}_{\rm ac} = F_{\rm ac}^{||}\hat{\mathbf{x}}$, to the dc drive. We measure the time average of the velocity per particle in the dc drift direction, $\langle V_x \rangle = N_m^{-1} \sum_{i=1}^{N_m} \mathbf{v}_i \cdot \hat{\mathbf{x}}$, where $\mathbf{v}_i$ is the velocity of particle i. We define the mobility as $M = \langle V_x \rangle / \langle V_x^0 \rangle$, where $\langle V_x^0 \rangle$ is the obstacle-free drift velocity so that, in the free flow limit, $M = 1.0$. After the drive is applied, there is a transient time during which the mobilities settle to a stationary state, so we wait 10^7 simulation time steps, longer than any of the transient times, before taking measurements. Our results are robust for varied system sizes, except that in very small samples ($L \leq 20$) particles are more likely to become trapped in periodic orbits, giving higher mobilities.

Results.—In Fig. 1(a), we illustrate the positions of the particles and obstacles in a steady state with $F_{\rm dc} = 0.05$, $\phi_{\rm tot} = 0.275$, and $\phi_{\rm obs} = 0.1256$ under a transverse drive $F_{\rm ac}^{\perp} = 0.5$ in the low-frequency limit of $\omega = 10^{-7}$, where the mobility is very small, $M = 0.01$. The particles assemble into high-density clogged regions separated by large void areas. There are slow particle rearrangements but little net motion in the dc drift direction, so the system is effectively transitioning between different clogged configurations. At $\omega = 10^{-4}$ in Fig. 1(b), the mobility reaches its maximum value of $M = 0.27$. In this partially fluidized state, the clustering is reduced compared to lower frequencies. For the high frequency of $\omega = 10^{-1}$ in Fig. 1(c), a completely frozen clogged state with $M = 0$ appears. In Fig. 1(d), when $\omega = 10^{-1}$ but the obstacle density is reduced to $\phi_{\rm obs} = 0.047$, we find a flowing state.

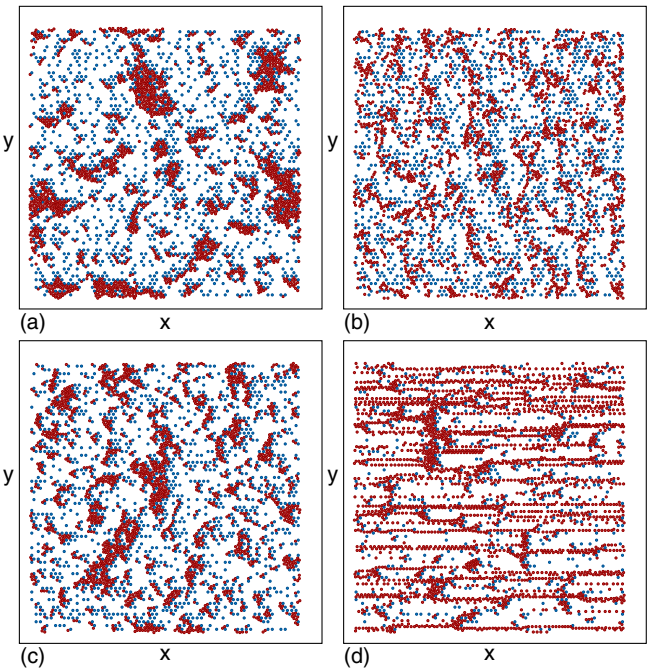

FIG. 1. Locations of particles (red) and obstacles (blue) for a system with $\phi_{\rm tot} = 0.275$ and an x-direction drift force of $F_{\rm dc} = 0.05$ under a transverse ac drive of magnitude $F_{\rm ac}^{\perp} = 0.5$ for different ac frequencies ω. (a) A low-mobility creeping clogged state with $M = 0.01$ at $\omega = 10^{-7}$ and $\phi_{\rm obs} = 0.1256$. (b) A high-mobility fluidized state with $M = 0.27$ at $\omega = 10^{-4}$ and $\phi_{\rm obs} = 0.1256$. (c) A frozen clogged state with $M = 0$ at $\omega = 10^{-1}$ and $\phi_{\rm obs} = 0.1256$. (d) A flowing state at $\omega = 10^{-1}$ and $\phi_{\rm obs} = 0.047$.

In Fig. 2(a), we plot M versus obstacle density $\phi_{\rm obs}$ for a system with $\phi_{\rm tot} = 0.275$ for zero ac drive and for $\omega = 10^{-4}$ ac drives that are transverse, $F_{\rm ac}^{\perp} = 0.5$, or longitudinal, $F_{\rm ac}^{||} = 0.5$. A clogged state with $M = 0$ appears for $\phi_{\rm tot} > 0.115$ under no ac drive, for $\phi_{\rm tot} > 0.2$ under transverse ac driving, and for $\phi_{\rm tot} > 0.155$ under longitudinal driving. For $\phi_{\rm obs} < 0.07$, M is the lowest under the transverse ac drive. In the inset in Fig. 3(a), we plot a dynamic phase diagram as a function of $\phi_{\rm obs}$ versus $\phi_{\rm tot}$ indicating the clogging transition lines $\phi_c^{\rm dc}$ for zero ac drive and $\phi_c^{\rm ac}$ for $F_{\rm ac}^{\perp} = 0.275$ and $\omega = 10^{-4}$. In the area between the two lines, the ac drive unclogs the system. At high $\phi_{\rm tot}$, both thresholds decrease upon approaching the crystallization or jamming transition near $\phi_{\rm tot} = 0.9$. Figures 1(a)–1(c) show the ac unclogged region at $\phi_{\rm tot} = 0.275$ and $\phi_{\rm obs} = 0.1256$, while Fig. 1(d) shows a region that is always unclogged. The extent of the ac unclogged region depends on the ac

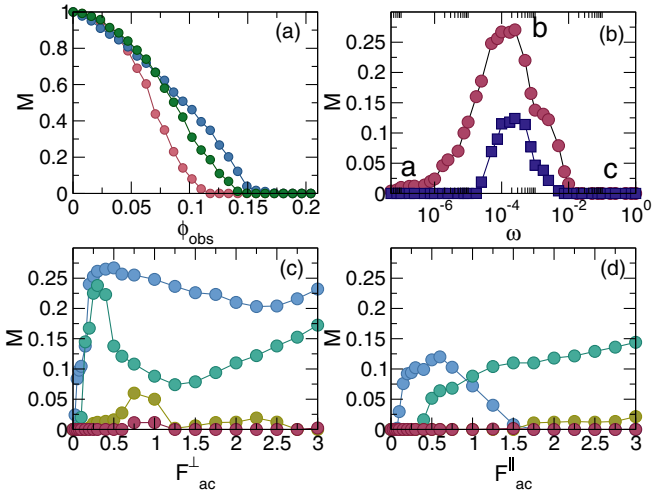

FIG. 2. (a) Mobility M versus obstacle density ϕ_{obs} for $\phi_{tot} = 0.275$ at $F^{\perp}_{ac} = F^{||}_{ac} = 0$ (pink), where $M = 0$ for $\phi_{obs} > 0.115$; at $F^{\perp}_{ac} = 0.5$ and $\omega = 10^{-4}$ (blue), where $M \approx 0$ for $\phi_{obs} > 0.195$; and at $F^{||}_{ac} = 0.5$ and $\omega = 10^{-4}$ (green), where $M \approx 0$ for $\phi_{obs} > 0.155$. (b) M versus ac frequency ω for the system in Figs. 1(a)–1(c) at $\phi_{tot} = 0.275$, $\phi_{obs} = 0.1256$, and $F_{ac} = 0.5$ for transverse (pink circles) and longitudinal (blue squares) ac driving, showing a clogged state at low and high frequencies and an intermediate frequency flowing state. The letters a, b, and c mark the frequencies at which the images in Figs. 1(a)–1(c) were obtained. (c) M versus $F^{\perp}_{ac}$ for the system in (b) under transverse driving with $\omega = 10^{-4}$ (blue), 10^{-3} (green), 10^{-2} (gold), and 10^{-1} (red). (d) M versus $F^{||}_{ac}$ at the same frequencies as in (c) under longitudinal driving.

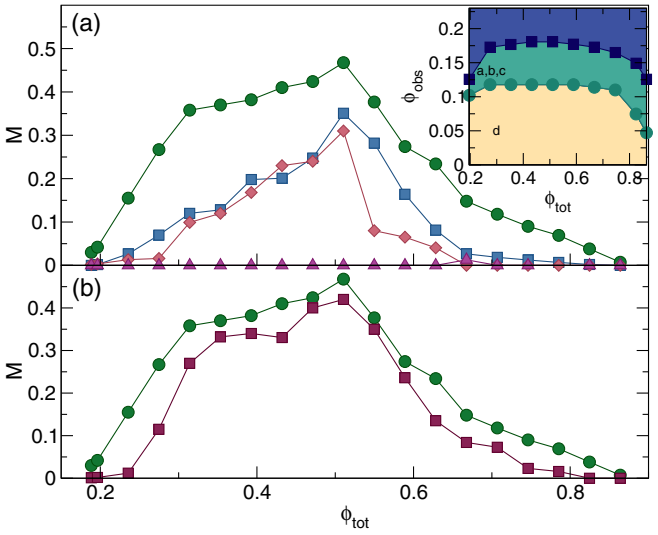

FIG. 3. (a) M versus ϕ_{tot} for $\phi_{obs} = 0.1256$ and $F^{\perp}_{ac} = 0.5$ at $\omega = 5.0 \times 10^{-6}$ (blue squares), 10^{-4} (green circles), 10^{-2} (pink diamonds), and 10^{-1} (magenta triangles). M is the largest for $\omega = 10^{-4}$. Inset: Dynamic phase diagram as a function of ϕ_{obs} versus ϕ_{tot}. Circles, ϕ^{dc}_{c}; squares, ϕ^{ac}_{c} for $F^{\perp}_{ac} = 0.5$ and $\omega = 10^{-4}$. Yellow: Flowing state. Blue: Clogged state. Green: ac unclogged state. The letters a–d indicate the points where the images in Figs. 1(a)–1(d) were obtained. (b) M versus ϕ_{tot} in the same system for transverse (green circles) and longitudinal (red squares) ac driving at $\omega = 10^{-4}$. M is the largest for transverse ac driving.

frequency, and at the highest frequencies it decreases in width until both clogging curves coincide.

In Fig. 2(b), we plot M versus ac frequency ω for the system from Figs. 1(a)–1(c) with $\phi_{tot} = 0.275$ and $\phi_{obs} = 0.1256$ for transverse and longitudinal ac driving of magnitude $F_{ac} = 0.5$. We find a low-mobility state for $\omega < 10^{-6}$ and a zero-mobility state for $\omega \geq 10^{-2}$. The optimal mobility occurs at $\omega \approx 2.5 \times 10^{-4}$. Both directions of ac driving produce the same dynamic states, but longitudinal driving gives a narrower window of unclogged states and a substantially lower value of M. Additionally, the low-frequency states with $\omega < 10^{-5}$ are fully clogged with $M = 0$ for longitudinal driving but have a small finite mobility for transverse driving. These results show that there are two different types of clogged states separated by an intermediate fluidized state in which the mobility reaches its optimum value. Figure 2(b) also indicates that the transverse ac drive is more effective at reducing clogging over a wide range of frequencies.

In Fig. 2(c), we plot M versus $F^{\perp}_{ac}$ for a system with $\phi_{tot} = 0.275$ and $\phi_{obs} = 0.1256$ at the optimal frequency of $\omega = 10^{-4}$ and at $\omega = 10^{-3}$, 10^{-2}, and 10^{-1}. An optimal value of $F^{\perp}_{ac}$ maximizes M at each frequency. Figure 2(d) shows M versus $F^{||}_{ac}$ at the same frequencies. At $\omega = 10^{-4}$, M increases to a local maximum at $F^{||}_{ac} = 0.5$ and then decreases to $M = 0$ in the clogged state for $F^{||}_{ac} > 1.5$. Previous studies of particles moving over random obstacles under a purely dc drive have shown that negative differential conductivity or a zero-mobility state can appear at high dc drives [39–42]. We find a similar effect under large longitudinal ac drives so that, in general, a clogged state appears for high $F^{||}_{ac}$. For $\omega = 10^{-3}$ in Fig. 2(d), M increases monotonically with $F^{||}_{ac}$; however, for much larger $F^{||}_{ac}$ (not shown), M decreases again. Transverse ac driving generally produces higher M by permitting the particles to move around obstacles, whereas longitudinal ac driving pushes the particles toward the obstacles and reduces M.

In Fig. 3(a), we plot M versus ϕ_{tot} for samples with $\phi_{obs} = 0.1256$ and $F^{\perp}_{ac} = 0.5$ at $\omega = 5.0 \times 10^{-6}$, 10^{-4}, 10^{-2}, and 10^{-1}. M is always small at low ϕ_{tot}, increases to a local maximum at $\phi_{tot} = 0.5$, and decreases to zero as ϕ_{tot} approaches $\phi_{tot} = 0.85$, the density of the crystallized solid [38,43]. We find the highest mobility for $\omega = 10^{-4}$, particularly for $0.66 < \phi_{tot} < 0.85$ where $M \approx 0$ for $\omega = 10^{-2}$ and 10^{-1}. In Fig. 3(b), we show M versus ϕ_{tot} at $\omega = 10^{-4}$ for transverse and longitudinal ac driving. A local maximum in M appears at $\phi_{tot} = 0.5$, and M is the largest under transverse ac driving for all ϕ_{tot}. The shape of M matches the clogging behavior of the phase diagram in

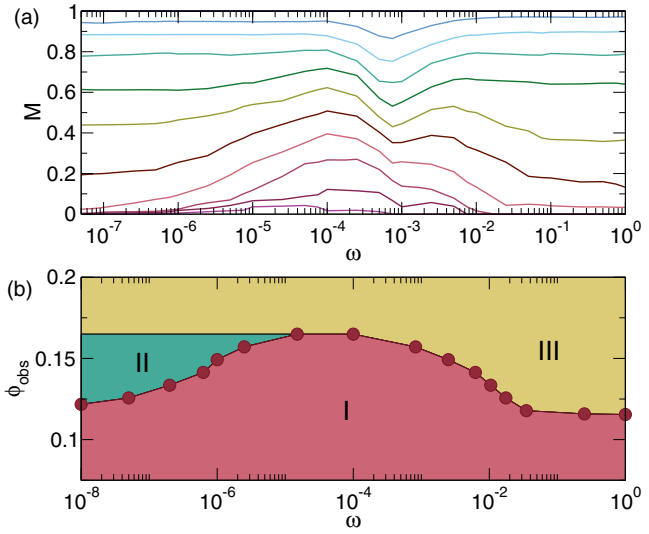

FIG. 4. (a) M versus ω for samples with $\phi_{tot} = 0.275$ and $F_{ac}^{\perp} = 0.5$ at $\phi_{obs} = 0.00157$, 0.031416, 0.047124, 0.062831, 0.07754, 0.09424, 0.1099, 0.1256 [also shown in Fig. 2(b)], 0.14137, and 0.157, from top to bottom. (b) Dynamic phase diagram as a function of ϕ_{obs} versus ω for $F_{ac}^{\perp} = 0.5$. I: flowing fluidized state; II: creeping clogged state; III: frozen clogged state.

the inset in Fig. 3(a). In Fig. 3(a), we show slices through the phase diagram in the ac unclogged region at $\phi_{obs} = 0.1256$ and varied ϕ_{tot}, where the clogging is fragile against the application of an ac drive.

In Fig. 4(a), we plot M versus ω in samples with $\phi_{tot} = 0.275$ and $F_{ac}^{\perp} = 0.5$ at $\phi_{obs} = 0.00157$ to 0.157. For $\phi_{obs} > 0.1099$, the system reaches a fully clogged state with $M = 0$. We define the clogging onset ϕ_c^{ac} as the point at which $M < 0.02$. A local maximum in M appears near $\omega = 2.5 \times 10^{-4}$ and shifts to slightly lower frequencies as ϕ_{obs} decreases. A local minimum near $\omega = 10^{-3}$ develops when $\phi_{obs} < 0.1099$ and shifts to lower frequencies with decreasing ϕ_{obs}. The local extrema are correlated with characteristic length scales. At the local maximum for $\phi_{obs} = 0.1256$, the distance $d_\tau = \omega^{-1} dt(F_{ac}^{\perp}/\sqrt{2} + F_{dc})$ a particle moves during one ac cycle matches the average spacing $l_{obs} = 1/\sqrt{\phi_{obs}}$ between obstacles. As l_{obs} decreases for increasing ϕ_{obs}, the maximum in M shifts to lower frequencies. The local minimum for $\phi_{obs} < 0.1099$ corresponds to the frequency at which d_τ matches the minimum transverse surface-to-surface obstacle spacing $d_{min} - 2R_d$, where the particles preferentially collide with the obstacles instead of moving around them. The two characteristic frequencies are separated by a factor of 10, since $F_{ac}^{\perp}/F_{dc} = 10$.

Based on the data in Fig. 4(a), in Fig. 4(b) we construct a dynamic phase diagram as a function of ϕ_{obs} versus ω for samples with $F_{ac}^{\perp} = 0.5$ showing phases I (flowing fluidized state), II (creeping clogged state), and III (frozen clogged state). For $\phi_{obs} > 0.165$, the spacing between obstacles becomes so small that the system is in a frozen state for all values of ω. The fluidized state is of maximum extent between $\omega = 10^{-5}$ and $\omega = 10^{-4}$. At higher ϕ_{tot} the ac drive unclogs the system, while at lower ϕ_{tot} in phase I the lower-mobility regimes are a vestige of the high- and low-frequency clogging behaviors from phases II and III. Longitudinal ac driving produces similar dynamic phases, except the extent of phase I is reduced.

Our results are similar to recent experiments on the viscosity of vibrated granular matter, where there is a jammed state at low frequencies, a low-viscosity fluid state at intermediate frequencies, and a reentrant jammed state at high frequencies [37]. Other granular studies have found optimal frequencies for dynamic resonances, where the speed of sound is minimized at intermediate frequencies when the grains are the least jammed [44].

Summary.—We examine the clogging and flow of particles through random obstacle arrays under a dc drift and a transverse or longitudinal ac drive. At zero ac driving, the system clogs above a well-defined obstacle density. When ac driving is added, the clogging transition shifts to much higher obstacle densities. For large obstacle densities, we find a low-frequency creeping clogged state where the particles rearrange from one clogged configuration to another with nearly zero drift mobility. At intermediate frequencies, a high-mobility fluidized state forms, while, at high frequencies, a zero-mobility frozen clogged state appears, giving an optimal mobility at intermediate frequencies. The mobility is also nonmonotonic when the ac amplitude is varied at a fixed frequency. Transverse ac driving is generally more effective at increasing the mobility than longitudinal ac driving. For a fixed ac amplitude and frequency the mobility is maximum at an optimal disk density, while for high disk densities a low-mobility jammed state emerges. At low obstacle densities, the system is always flowing; however, transverse ac driving produces a resonant frequency with reduced flow when the transverse oscillations match the minimum obstacle spacing. We map a dynamic phase diagram showing the locations of the flowing, creeping clogged, and frozen clogged states.

Our results suggest that ac driving could be used to avoid clogging and optimize particle flows in disordered media and offer a technique for particle species separation through selective clogging when the species have different frequency-dependent mobilities. These results can be generalized for controlling flows in a wide class of collectively interacting particle systems in heterogeneous environments, including colloids, bubbles, granular matter, vortices in superconductors, and Skyrmions in chiral magnets.

This work was carried out under the auspices of the National Nuclear Security Administration of the U.S. Department of Energy at Los Alamos National Laboratory (LANL) under Contract No. DE-AC52-06NA25396 and through the LANL Laboratory Directed Research and Development program.

[1] L. M. McDowell-Boyer, J. R. Hunt, and N. Sitar, Water Resour. Res. **22**, 1901 (1986).
[2] D. C. Mays and J. R. Hunt, Environ. Sci. Technol. **39**, 577 (2005).
[3] L. R. Huang, E. C. Cox, R. H. Austin, and J. C. Sturm, Science **304**, 987 (2004).
[4] P. Tierno, T. H. Johansen, and T. M. Fischer, Phys. Rev. Lett. **99**, 038303 (2007).
[5] Z. Li and G. Drazer, Phys. Rev. Lett. **98**, 050602 (2007).
[6] R. Zhang and J. Koplik, Phys. Rev. E **85**, 026314 (2012).
[7] J. McGrath, M. Jimenez, and H. Bridle, Lab Chip **14**, 4139 (2014).
[8] H. M. Wyss, D. L. Blair, J. F. Morris, H. A. Stone, and D. A. Weitz, Phys. Rev. E **74**, 061402 (2006).
[9] F. Chevoir, F. Gaulard, and N. Roussel, Europhys. Lett. **79**, 14001 (2007).
[10] G. C. Agbangla, P. Bacchin, and E. Clement, Soft Matter **10**, 6303 (2014).
[11] H. T. Nguyen, C. Reichhardt, and C. J. O. Reichhardt, Phys. Rev. E **95**, 030902(R) (2017).
[12] H. Peter, A. Libal, C. Reichhardt, and C. J. O. Reichhardt, Sci. Rep. **8**, 10252 (2018).
[13] R. L. Stoop and P. Tierno, arXiv:1712.05321.
[14] S. Redner and S. Datta, Phys. Rev. Lett. **84**, 6018 (2000).
[15] N. Roussel, T. L. H. Nguyen, and P. Coussot, Phys. Rev. Lett. **98**, 114502 (2007).
[16] C. Barré and J. Talbot, J. Stat. Mech. 2017, 043406
[17] O. Chepizhko, E. G. Altmann, and F. Peruani, Phys. Rev. Lett. **110**, 238101 (2013).
[18] C. Bechinger, R. Di Leonardo, H. Löwen, C. Reichhardt, G. Volpe, and G. Volpe, Rev. Mod. Phys. **88**, 045006 (2016).
[19] A. Morin, N. Desreumaux, J.-B. Caussin, and D. Bartolo, Nat. Phys. **13**, 63 (2017).
[20] Cs. Sándor, A. Libál, C. Reichhardt, and C. J. O. Reichhardt, Phys. Rev. E **95**, 032606 (2017).
[21] C. Reichhardt and C. J. O. Reichhardt, Rep. Prog. Phys. **80**, 026501 (2017).
[22] K. To, P.-Y. Lai, and H. K. Pak, Phys. Rev. Lett. **86**, 71 (2001).
[23] I. Zuriguel, L. A. Pugnaloni, A. Garcimartín, and D. Maza, Phys. Rev. E **68**, 030301(R) (2003).
[24] D. Chen, K. W. Desmond, and E. R. Weeks, Soft Matter **8**, 10486 (2012).
[25] I. Zuriguel *et al.*, Sci. Rep. **4**, 7324 (2014).
[26] R. C. Hidalgo, A. Goñi-Arana, A. Hernández-Puerta, and I. Pagonabarraga, Phys. Rev. E **97**, 012611 (2018).
[27] C. Mankoc, A. Garcimartín, I. Zuriguel, D. Maza, and L. A. Pugnaloni, Phys. Rev. E **80**, 011309 (2009).
[28] C. Lozano, G. Lumay, I. Zuriguel, R. C. Hidalgo, and A. Garcimartín, Phys. Rev. Lett. **109**, 068001 (2012).
[29] A. Janda, D. Maza, A. Garcimartín, E. Kolb, J. Lanuza, and E. Clément, Europhys. Lett. **87**, 24002 (2009).
[30] J. A. Dijksman, G. H. Wortel, L. T. H. van Dellen, O. Dauchot, and M. van Hecke, Phys. Rev. Lett. **107**, 108303 (2011).
[31] M. Griffa, E. G. Daub, R. A. Guyer, P. A. Johnson, C. Marone, and J. Carmeliet, Europhys. Lett. **96**, 14001 (2011).
[32] H. Lastakowski, J.-C. Géminard, and V. Vidal, Sci. Rep. **5**, 13455 (2015).
[33] K. To and H.-T. Tai, Phys. Rev. E **96**, 032906 (2017).
[34] G. A. Patterson, P. I. Fierens, F. S. Jimka, P. G. König, A. Garcimartín, I. Zuriguel, L. A. Pugnaloni, and D. R. Parisi, Phys. Rev. Lett. **119**, 248301 (2017).
[35] D. Helbing, I. J. Farkas, and T. Vicsek, Phys. Rev. Lett. **84**, 1240 (2000).
[36] J. M. Pastor, A. Garcimartín, P. A. Gago, J. P. Peralta, C. Martín-Gómez, L. M. Ferrer, D. Maza, D. R. Parisi, L. A. Pugnaloni, and I. Zuriguel, Phys. Rev. E **92**, 062817 (2015).
[37] A. Gnoli, L. de Arcangelis, F. Giacco, E. Lippiello, M. P. Ciamarra, A. Puglisi, and A. Sarracino, Phys. Rev. Lett. **120**, 138001 (2018).
[38] C. Reichhardt and C. J. O. Reichhardt, Soft Matter **10**, 2932 (2014).
[39] S. Leitmann and T. Franosch, Phys. Rev. Lett. **111**, 190603 (2013).
[40] U. Basu and C. Maes, J. Phys. A **47**, 255003 (2014).
[41] O. Bénichou, P. Illien, G. Oshanin, A. Sarracino, and R. Voituriez, Phys. Rev. Lett. **113**, 268002 (2014).
[42] M. Baiesi, A. L. Stella, and C. Vanderzande, Phys. Rev. E **92**, 042121 (2015).
[43] A. J. Liu and S. R. Nagel, Annu. Rev. Condens. Matter Phys. **1**, 347 (2010).
[44] C. J. O. Reichhardt, L. M. Lopatina, X. Jia, and P. A. Johnson, Phys. Rev. E **92**, 022203 (2015).